

The sdA problem – III. Hundreds of new extremely low-mass white dwarfs and their precursors from *Gaia* astrometry

Ingrid Pelisoli^{1*}, Keaton J. Bell^{2,3}, S. O. Kepler¹, D. Koester⁴

¹*Instituto de Física, Universidade Federal do Rio Grande do Sul, 91501-900, Porto-Alegre, RS, Brazil*

²*Max-Planck-Institut für Sonnensystemforschung (MPS), Justus-von-Liebig-Weg 3, 37077 Göttingen, Germany*

³*Department of Physics and Astronomy, Stellar Astrophysics Centre, Aarhus University, Ny Munkegade 120, 8000 Aarhus C, Denmark*

⁴*Institut für Theoretische Physik und Astrophysik, Universität Kiel, D-24098, Kiel, Germany*

Accepted XXX. Received YYY; in original form ZZZ

ABSTRACT

The nature of the sdA stars—cool hydrogen-rich objects with spectroscopic surface gravities intermediate between main sequence and canonical mass white dwarfs—has been elusive since their discovery in Sloan Digital Sky Survey Data Release 12 spectra. The two main hypotheses to explain these objects are A/F stars in the halo with an overestimated $\log g$, or extremely low-mass white dwarfs and their precursors, i.e., ELMs and pre-ELMs. In this work, we analyse 5 688 sdAs previously identified in the Sloan Digital Sky Survey using *Gaia* DR2 data. We confirm that 277 of them have radii smaller than the main sequence, even allowing for very low metallicity. These are likely (pre-)ELMs given their spectral class, although the number of stars in our high-likelihood (pre-)ELM sample may be 20 per cent lower depending on extinction. These identifications increase the number of known (pre-)ELMs threefold, and the demonstration that a sizeable fraction of the sdA stars must be (pre-)ELMs helps to resolve the recent debate about their physical nature.

Key words: subdwarfs – white dwarfs – binaries: general – stars: evolution

1 INTRODUCTION

The spectroscopic class of subdwarf A stars (sdAs) was proposed by Kepler et al. (2016) to refer to thousands of hydrogen-rich objects in the Sloan Digital Sky Survey (SDSS) whose surface gravities derived from their spectra could not be explained by single-star evolution models. They show temperatures below the zero-age horizontal branch (ZAHB), $7\,000 \lesssim T_{\text{eff}} < 20\,000$ K (most $\lesssim 10\,000$ K), and $\log g$ intermediate between main sequence A stars and hydrogen-atmosphere (DA) white dwarfs resulting from single evolution, $4.5 \lesssim \log g \lesssim 6.0$. They were unveiled among stars identified as O, B, and A type by the SDSS pipeline. Given the saturation limit of the SDSS at $g \approx 14.0$, early-type main sequence stars should be above it unless they are more distant than ≈ 8 kpc, or essentially in the halo, given that SDSS observes mostly outside of the disc. As the halo is over 10 Gyr old and the main sequence lifetimes of these spectral classes is shorter than 1.5 Gyr, we do not expect a scattered large population of early-type stars in SDSS.

The initial suggestion of Kepler et al. (2016) was

that the sdAs could be extremely-low mass white dwarfs (ELMs) missed by the selection criteria of the ELM Survey (Brown et al. 2010; Kilic et al. 2011; Brown et al. 2012; Kilic et al. 2012; Brown et al. 2013; Gianninas et al. 2015; Brown et al. 2016). ELMs show masses below the single-star evolution limit for white dwarfs of $M \approx 0.3 M_{\odot}$ ($\log g \approx 6.0$). The Universe is not old enough for low mass stars to have evolved off the main sequence and turned into $M \lesssim 0.3 M_{\odot}$ white dwarfs (e.g. Kilic et al. 2007). However, over 50 per cent of stars with $M \gtrsim 1 M_{\odot}$ are in binaries (Duchêne & Kraus 2013), and about 25 per cent are close enough to interact (Willems & Kolb 2004), potentially leading to a common envelope phase. The friction between the pair of stars and the envelope can lead to envelope ejection, causing significant mass loss and bringing the binary stars closer together. This is believed to be the main channel of ELM formation (e.g., Marsh et al. 1995; Nelemans et al. 2001).

The ELM Survey selected mostly hot ($T \gtrsim 10\,000$ K), $M \gtrsim 0.15 M_{\odot}$ ELMs. Moreover, they considered the detection of a close binary companion as a requirement for a clear ELM classification (Brown et al. 2016). Whereas common-envelope evolution is thought to be the main for-

* E-mail: ingrid.pelisoli@ufrgs.br

mation channel for ELMs, alternative formation scenarios include the merger of the inner binary in a hierarchical triple system (Vos et al. 2018), supernova stripping (Wang & Han 2009), and mass ejection caused by a massive planet (Nelemans & Tauris 1998). Therefore, the existence of single ELMs should not be ruled out. The ELMs can give us important clues as to the evolution of compact binary systems and of hierarchical triple systems, which is still poorly understood (e.g. Postnov & Yungelson 2014; Toonen et al. 2016), hence an unbiased-sample would be a valuable asset to testing evolution and population synthesis models.

The ELM explanation for the sdAs was questioned by Brown et al. (2017) and Hermes et al. (2017). Hermes et al. (2017) relied on the radial velocities estimated from SDSS subspectra and concluded that the vast majority of the sdAs published by Kepler et al. (2016) (> 99 per cent) were not in close binaries, and therefore that they could not be ELMs. Other formation channels such as merging were excluded due to the low proper motion of most of the sdAs published in Kepler et al. (2016). Brown et al. (2017) suggested that sdAs were predominantly metal-poor A/F main sequence stars in the halo, arguing that the number of sdAs was far too large compared to the predicted number of cool ELMs given the density of objects estimated from the known sample. They also studied six eclipsing binaries in the sample, and found their radii to be too large for compact objects. The possibility that the objects were in the pre-ELM phase, before the star reaches the cooling branch and still shows an extended radius, was not seriously considered, perhaps because the lifetimes in those phases are short. Brown et al. (2017) also suggested that the use of pure-hydrogen models caused the $\log g$ values of Kepler et al. (2016) to be overestimated.

In Pelisoli et al. (2018b), we showed that metallicity could not be responsible for a systematic overestimate of $\log g$. Some values of $\log g$ could even be underestimated by the pure-hydrogen models. Moreover, we found no dependence with metallicity for the difference between our $\log g$ values and those estimated by the SEGUE stellar parameter pipeline (SSPP, Lee et al. 2008). Importantly, it became clear that the sdAs were composed of overlapping stellar populations, given a bi-modal distribution in $(g - z)$. This result was corroborated by Bell et al. (submitted to A&A), who found that the sdAs show varied pulsation spectra that cannot be explained with a single population. We obtained another interesting result in Pelisoli et al. (2018a) by comparing the $\log g$ obtained from SDSS spectra with values derived from X-shooter spectra. The SDSS values for the four stars observed were larger by 1 dex, which could be explained by the lack of spectral coverage below 3700 Å and low resolution in the SDSS spectra, since the widths of the lines show little dependence on $\log g$ for temperatures in the sdA range. This could potentially explain the inconsistency raised by Brown et al. (2017).

Clearly, the SDSS spectra and colours are not enough to uniquely determine the nature of the sdA stars. They could be binary byproducts, holding the potential to shed light on the evolution of multiple systems, or main sequence stars in the halo, which could illuminate the structure and formation history of the Galaxy. Resolving their nature is therefore advantageous in both aspects. With parallax measurements from data release 2 of *Gaia*, we can place con-

straints on the radii of these objects, making their nature clearer. In this work, we explore the nature of the sdAs in light of *Gaia* DR 2 data. In particular, we seek to identify sdAs that must be (pre-)ELMs based on radius constraints from *Gaia* astrometry.

2 DATA ANALYSIS

We focused our analysis on objects from sample A of Pelisoli et al. (2018b), which were selected among stars with SDSS pipeline classifications of O, B, and A for which we obtained good spectroscopic fits (38 850 objects). We also analyse objects in tables 1 and 2 of that work in particular. The former are objects whose SDSS spectra yield $\log g > 5.5$ when fit with solar-abundance spectral models. The latter were objects found to be more likely (pre-)ELMs than main sequence stars given a probabilistic analysis that took into account the $g - z$ colours, spatial velocities (U, V, W), and the fitted $\log g$ values compared to both single (Bertelli et al. 2008, 2009) and binary evolution models (Istrate et al. 2016).

We retrieved their coordinates (α, δ) , parallaxes (π) , proper motions $(\mu_\alpha$ and $\mu_\delta)$, and magnitudes in the G , G_{BP} and G_{RP} filters from the *Gaia* DR2 catalogue using the coordinates from SDSS and a 3" search radius. For 490 objects there were multiple identifications within this radius; we selected the *Gaia* source closer to the SDSS coordinates, being left with identifications for 38 825 objects within 3". All but two of the unmatched sources correspond to spectra taken at the position of diffraction rays of bright stars by the SDSS. One of the remaining two could be recovered with a 5" radius, but the other returned no match even with a 15" radius. We subtracted the zero-point of $-29 \mu\text{as}$ from the parallaxes (Lindegren et al. 2018) of all matched objects. This zero-point was determined from quasars, which have similar colours to white dwarfs and A-type stars, hence it should be adequate to our sample. There is, however, a dependence of this zero-point with colour, and it can be larger for cooler objects (see e.g. Zinn et al. 2018). We selected from the corrected sample only the ones with a positive parallax ($30\,792$), and restricted the analysis to objects showing $\pi \geq 3\sigma_\pi$ ($6\,832$). Finally, we removed double identifications (objects with more than one observation in the SDSS, with slightly different coordinates). This left $5\,742$ unique identifications with a reliable π .

We estimated the distance d , absolute magnitude M_G , bolometric magnitude M_{bol} , luminosity $\log(L/L_\odot)$, and radius R/R_\odot for each object with a Monte Carlo simulation, taking into account the uncertainties in the value of π . The uncertainties in the G magnitude, in the extinction correction A_G , and in T_{eff} (assumed to be equal to the external uncertainty of 5 per cent) are also propagated. Expected values were taken to be the median of the distribution, whereas upper and lower uncertainties were taken to be the 16th and 84th percentiles, yielding an interval of confidence of 68 per cent. The distance d was calculated from the distribution of $(\pi')^{-1}$, where π' is the parallax corrected for the zero point. The absolute magnitude for each source was calculated as

$$M_G = G - A_G + 5 \log \pi' + 5, \quad (1)$$

where the extinction correction was also retrieved from the

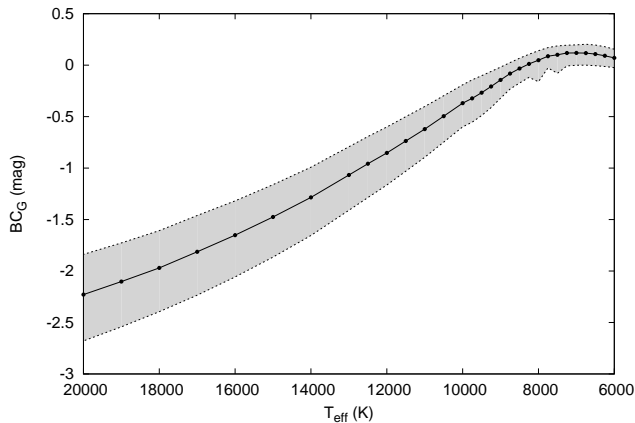


Figure 1. The black points show the average values of the bolometric correction to M_G for each T_{eff} (Jordi et al. 2010). They give a smooth function represented by the solid line, hence the bolometric correction can be estimated from interpolation given the T_{eff} . The dashed lines represent the minimum and maximum value for each T_{eff} .

Gaia DR2 catalogue where available. We applied the bolometric corrections given in table 12 of Jordi et al. (2010) to obtain M_{bol} . As the external uncertainty in the $\log g$ that we derived from SDSS spectra is quite high (about 0.5 dex, see discussion in Pelisoli et al. 2018a) and we do not have high resolution spectra to accurately determine the metallicity, we assume the average bolometric correction given the effective temperature (which has an uncertainty smaller than 5 per cent when derived from the SDSS spectra, see Pelisoli et al. 2018b,a), with the uncertainty taken to be the difference between either the minimum or the maximum value and the average — whichever was larger. As can be seen in Fig. 1, the bolometric correction does not have a large dependence on $\log g$ and metallicity in the temperature range of the sdAs, so the uncertainties from this method are only on the order of 0.5 mag, still they were also propagated in our simulation. Using the bolometric magnitude, we calculated $\log(L/L_{\odot})$ from

$$\log\left(\frac{L}{L_{\odot}}\right) = \frac{4.75 - M_{\text{bol}}}{2.5}. \quad (2)$$

We computed the radius of each object in two different ways. First, we used the Stefan-Boltzmann law relating L , T_{eff} and R . The main source of uncertainty in this case is the bolometric correction. To obtain a second estimate independent of the bolometric correction, we have also computed the radii using the solid angle obtained as part of our photometric fit to each object. As the spectroscopic fit can show degenerate solutions with similar χ^2 , we first fit the photometry assuming a fixed $\log g = 4.5$ so that we can select the spectroscopic solution whose temperature is consistent with the photometry. The ratio between the observed and modelled photometric brightness is related to the solid angle, which is proportional to $(R/d)^2$. Hence, the radius can be estimated given the distance. The main uncertainty in this case is the extinction correction. We applied the full-correction from the maps of Schlegel et al. (1998), which have a resolution of only $4'$, to the *ugriz* magnitudes. The radius estimates from the two methods were not consis-

tent within 3σ for only 54 objects. To avoid contamination, we removed these objects from the sample. Henceforth we use the estimate from the luminosity, which is independent from our fit to the SDSS photometry.

Given the *Gaia* five-parameter astrometric solutions, we have also computed the galactic coordinates X, Y, Z and spatial velocities U, V, W for each of our targets following Johnson & Soderblom (1987). Given that they are too faint to have radial velocity estimates from *Gaia*, we have relied on the radial velocities that we estimated from their SDSS spectra. Our estimates derived from the hydrogen lines show very good agreement with the estimates from the SDSS pipeline.

The radial velocity variations between SDSS subspectra of the objects in this sample were also analysed. These amplitudes were calculated with the approach described in Pelisoli et al. (2017), which was based on the work of Badenes & Maoz (2012). It consists of fitting a Gaussian to each of the Balmer lines in the normalized spectra to determine the line centre, and using this value to compute a radial velocity for each line. The radial velocity of the object at the epoch of the spectrum is calculated to be the average velocity over all the lines. We then calculate the difference between minimal and maximal velocities for each object, which is a proxy for the amplitude of radial velocity variation. We obtained good fits to the subspectra of 5375 objects in the sample.

3 RESULTS

The main explanations put forward for the sdAs are A/F main sequence stars in the halo (Brown et al. 2017), and (pre-)ELMs (Pelisoli et al. 2018b). The main difference between these two evolutionary classes is their radii. A/F main sequence stars show $R \gtrsim 0.6 R_{\odot}$, depending on T_{eff} , even for very low metallicity (e.g. $z \approx 10^{-4}$, see Fig. 2). With larger metallicity, the radius is larger because of the increase in opacity, which traps the photons for longer. The evolution off the main sequence also causes the radius to increase, due to thermal energy being released by the contracting nucleus. Hence, the zero age main sequence (ZAMS) radius for low metallicity is the conservative minimal radius for a main sequence star at a given T_{eff} . (Pre-)ELMs, on the other hand, have $R \lesssim 0.1 R_{\odot}$ during most of their evolution. The radius of a pre-ELM can nonetheless be larger, because of residual burning (e.g. the RR Lyra found by Pietrzyński et al. 2012). Although the time spent in these burning stages is short, the objects are much brighter, hence they have considerable chances of being detected (Pelisoli et al. 2018b). In short, (pre-)ELMs can show radii in an extensive range, but main sequence stars have a minimal radius.

We have used this minimal radius to investigate which objects in our sample could not be explained as main sequence stars. Using the radii estimated from the luminosities, we verified whether the radius of each star was smaller than the ZAMS at the estimated T_{eff} considering the 99 per cent confidence interval of our Monte Carlo simulation — i.e. 99 per cent of the simulated radii had to be below the minimum radius at the best-fit T_{eff} for it to be considered smaller than the ZAMS. From the sample with 5688 objects with radii agreeing between the two methods, we found

297 showing $R_{99\%} < R_{\text{ZAMS}}$. Objects with radii below the ZAMS cannot be main sequence stars. Considering their spectral class, they can only be explained as (pre-)ELMs, which are most likely byproducts of binary evolution. Removing canonical mass white dwarfs with spectral types other than A (e.g. with helium contamination or magnetic fields, which affect the $\log g$ estimate), we are left with 277 (pre-)ELMs. These objects are listed in Table 1. Three are previously known ELMs published by Brown et al. (2016), and 31 one were previously classified as white dwarfs (mostly by Kleinman et al. 2013), but only fitted with models with $\log g > 5.0$, whereas our grid extends down to $\log g = 3.5$.

Only a small fraction (~ 30 per cent) of the objects in our sample had extinction corrections available in *Gaia* DR2. Failing to correct extinction can cause the distances and radii to be underestimated. To estimate the effect of a lack of extinction correction, we made another calculation of radii obtaining the apparent G from the SDSS filters g and i , using the transformations of Evans et al. (2018) and correcting extinction in both SDSS filters following Schlegel et al. (1998). Considering these radii, 20 per cent of the (pre-)ELMs would have inconclusive radii. Given that the extinction map of Schlegel et al. (1998) has low resolution, as already mentioned above, we preferred to use the radii derived from *Gaia* parameters alone, but we caution that there is a 20 per cent uncertainty in the number of (pre-)ELMs because of unaccounted-for extinction.

The fraction of (pre-)ELMs among the sdAs with reliable parallax changes from 5.2 to 5.0, 5.3, and then 11.6 per cent for π larger than 4, 5, and 10 σ_π , respectively. We suggested in Pelisoli et al. (2018b) that at least ≈ 7 per cent of the sdAs were (pre-)ELMs. However, nearby stars are more likely to have high signal-to-noise parallax measurements, so we may be biased toward having (pre-)ELMs in our sample of astrometric sdAs, given the SDSS saturation limit. This bias explains the increase in confirmed (pre-)ELM fraction with signal-to-noise, and the complicated selection effects of this sample would need to be determined to assess the accurate fraction of sdAs that are (pre-)ELMs.

We find that the (pre-)ELMs in the reliable parallax sample show apparent magnitudes generally fainter than the remaining objects (see Fig. 3). White dwarfs are intrinsically fainter, so that even at relatively high G the parallax can be detected. Most of the remaining objects show a confidence interval for the radii spanning both above and below the main sequence, with only 483 objects showing the 99 per cent confidence level above the main sequence minimum. We cannot make any claims about the nature of the objects whose radii are not below the ZAMS; they are consistent with both the main sequence and with pre-ELMs, given the occurrence of burning stages that increase the pre-ELM radii up to above the main sequence, as mentioned above. For example, Liakos (2018) recently found a $0.07 M_\odot$ pre-ELM with a $1.0 R_\odot$ radius in an Algol-type binary.

In Fig. 4, we show the H-R diagram for our reliable π sample. Single and binary evolution models are overplotted. Remarkably, the position of the objects for which we determine the radius to be smaller than the main sequence agrees quite well with the binary evolution models of Istrate et al. (2016), providing further evidence that they are, in fact, ELMs and their precursors. These objects also lie below the

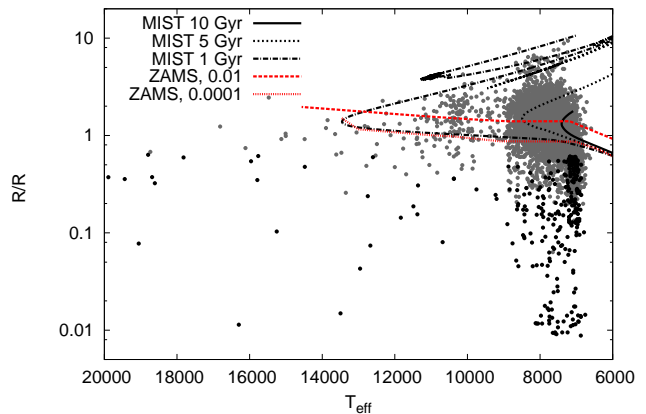


Figure 2. Radius as a function of T_{eff} for all objects with reliable parallax. The red lines show the zero-age main sequence (ZAMS) for the two indicated metallicities (Romero et al. 2015). The black lines show the radii from MIST isochrones (Dotter 2016; Choi et al. 2016) for $[\text{Fe}/\text{H}] = -4$. The objects showing radii smaller than the minimum main sequence radius, taking into account a 99 per cent confidence interval, are shown in black.

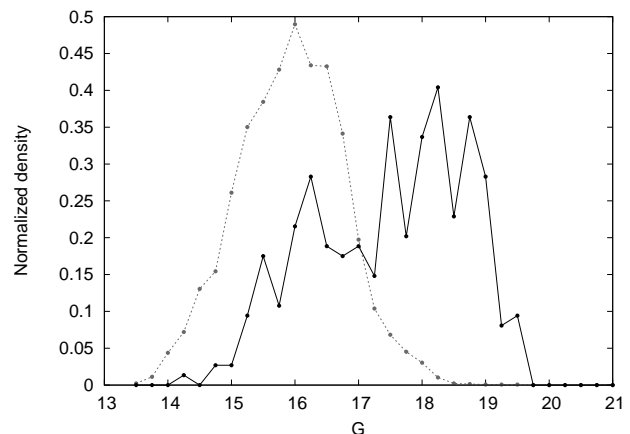


Figure 3. Number density of objects as a function of apparent magnitude G . The black solid line shows objects whose radii is smaller than main sequence, the grey dashed is for the remaining objects in the sample.

main sequence in the observational H-R diagram (colour-magnitude diagram), shown in Fig. 5.

Given their smaller-than-main-sequence radii, the distances of the (pre-)ELM objects are consistent with the Galactic disc, as we had already suggested in Pelisoli et al. (2018b). Objects with inconclusive radii extend to larger distances. Fig. 6 shows a diagram of Z as a function of $\rho = \sqrt{X^2 + Y^2}$. The (pre-)ELMs are all within 3 kpc. SDSS observed only 35 per cent of the sky, and only 40 per cent of white dwarfs were followed up spectroscopically with SDSS (Gentile Fusillo et al. 2015); accounting for this, the population is consistent with a thick disc with a scale height of 900 pc (Bland-Hawthorn & Gerhard 2016), as can be seen in the histogram of Fig 7. There is a noticeable bimodality in the Z distribution. This can partially be explained by the possible presence of canonical-mass white dwarfs in the

Table 1. (Pre-)ELMs and some possibly canonical mass white dwarfs identified in the sdA sample. Uncertainties in T_{eff} and $\log g$ are formal fitting errors obtained from the SDSS spectral fit. The radii were calculated from the luminosity derived from Gaia data and our spectroscopic T_{eff} . The complete Table is available online.

SDSS J	T_{eff} (K)	$\log g$	d (pc)	$\sigma_{d_{\text{upper}}}$	$\sigma_{d_{\text{lower}}}$	$R(R_{\odot})$	$\sigma_{R_{\text{upper}}}$	$\sigma_{R_{\text{lower}}}$
000316.15-050040.8	7016(19)	4.21(0.10)	1165	317	442	0.2013	0.0822	0.0475
000320.54-103758.4	7194(13)	4.44(0.04)	1708	249	288	0.4564	0.1029	0.0782
000720.18-023456.0	7594(33)	5.82(0.08)	109	6	6	0.0093	0.0014	0.0012
000758.17-024941.8	7650(29)	6.11(0.07)	106	3	3	0.0094	0.0012	0.0011
002105.91-024907.7	7153(42)	7.69(0.07)	117	4	4	0.0110	0.0014	0.0012
002543.80-104706.8	6919(35)	3.87(0.18)	1526	354	446	0.2652	0.0851	0.0558
002808.62+172911.2	7202(35)	4.20(0.13)	1251	382	552	0.1364	0.0639	0.0343
004001.42+005908.7	7391(34)	5.37(0.10)	128	7	7	0.0095	0.0014	0.0012
004233.28+001711.1	7117(21)	4.27(0.07)	1111	295	406	0.1911	0.0740	0.0444
005659.78+135447.1	7222(34)	4.48(0.12)	685	213	313	0.0595	0.0283	0.0151

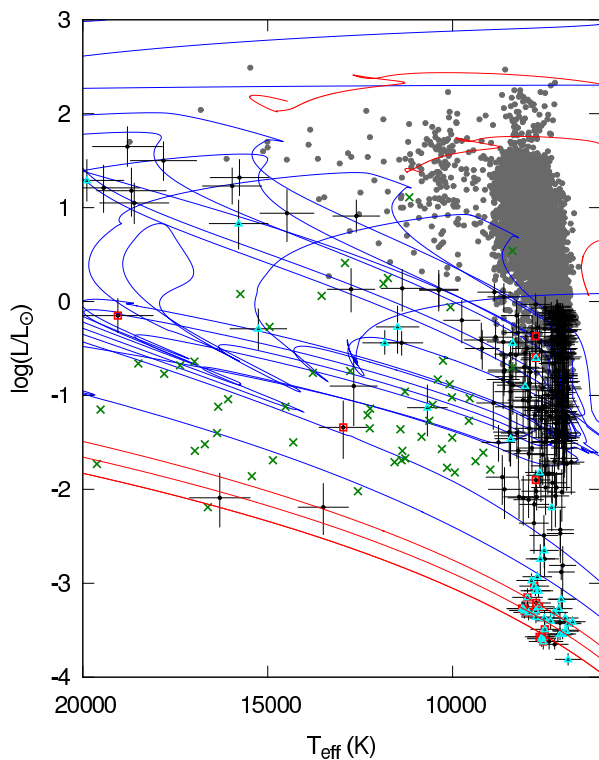


Figure 4. H-R diagram showing the whole reliable π sample as grey dots. The objects with radii smaller than main sequence assuming a 99 per cent confidence interval are shown in black, with error bars. Objects found to be most likely (pre-)ELMs from Pelisoli et al. (2018b) are marked with cyan triangles, while those with $\log g > 5.5$ are marked with red squares. Blue lines show the binary evolution models of Istrate et al. (2016) for $z = 0.01$ that take rotation into account, ranging from 0.182 (top) to $0.324 M_{\odot}$ (bottom). The location of the (pre-)ELMs agrees remarkably well with the region spanned by these models, with the exception of a few canonical-mass white dwarfs. Known ELMs in binaries from table 5 of Brown et al. (2016) are shown as green crosses for comparison. The red lines are single-evolution models computed with the LPCODE (Althaus et al. 2003) for low-metallicity ($z = 0.004$) stars with initial masses of 1.0 , 2.0 , and $3.0 M_{\odot}$ (from top to bottom).

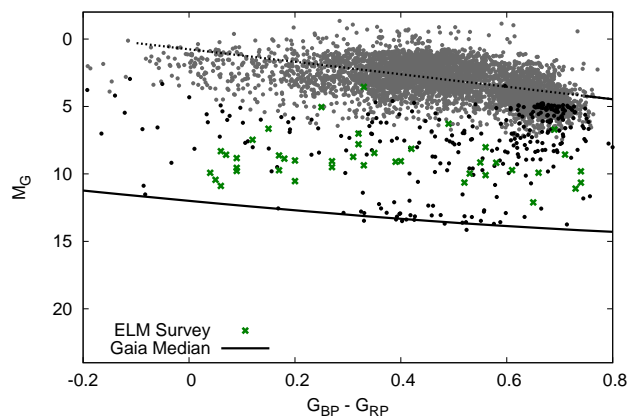


Figure 5. Absolute magnitude M_G and colour $G_{BP} - G_{RP}$. Extinction and reddening corrections from Gaia were applied when available. The red lines are the fiducial lines from fig. 8 of Gaia Collaboration et al. (2018), which show the position of the main sequence (top) and white dwarfs (bottom). The dashed portion was extrapolated. Colour coding for the dots is the same as in Fig. 4.

sample, which are intrinsically fainter than (pre-)ELMs and could account for the peak at smaller Z . However, a certain bimodality in the radii of detected (pre-)ELMs can also be explained in terms of their evolution. As previously stated, most of their lives is spent in the cooling sequence with $R \lesssim 0.1 R_{\odot}$, which increases the probability of detection at these small radii. On the other hand, the maximum distance at which a (pre-)ELM can be detected scales with its radius. From the models of Istrate et al. (2016), we obtained that the maximum observable volume becomes the dominant factor for the probability of detection at $R \gtrsim 0.2 R_{\odot}$. Therefore there are two regimes for (pre-)ELM detection: dominated by the large timescales (small radii), or dominated by brightness (large radii). As our initial sample selection took into account the SDSS spectral classification as main sequence A, B or O stars, it should be biased toward the large radii regime, because small radii objects would be most likely classified as white dwarfs by the SDSS pipeline.

The kinematics of the new (pre-)ELMs is harder to parse, as is shown in Fig. 8. The peak is consistent with

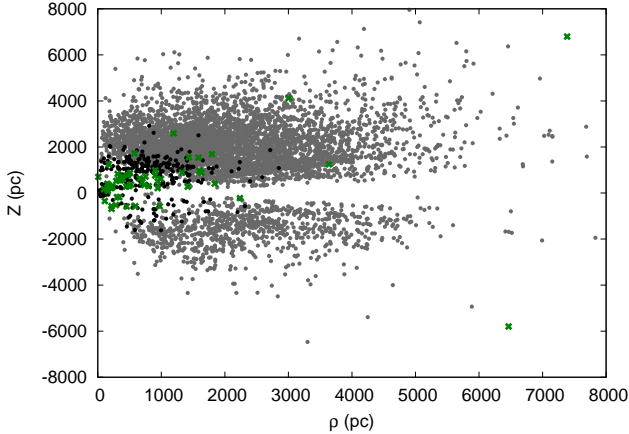


Figure 6. Diagram showing the disc height Z vs. the distance in the Galactic plane $\rho = \sqrt{X^2 + Y^2}$, with same colour coding as previous figures. There are more objects at $Z > 0$ and few close to the disk because of the SDSS coverage of the sky.

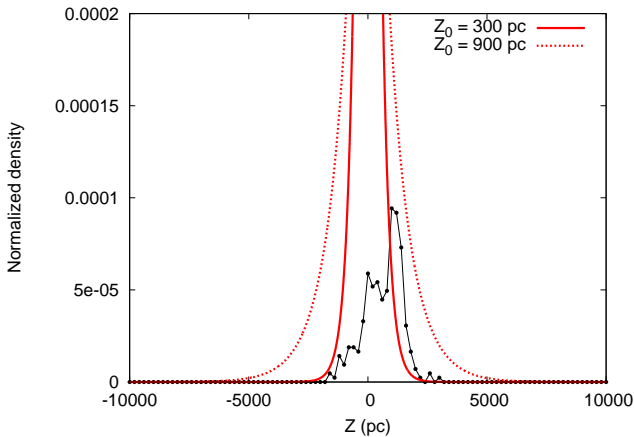


Figure 7. Distribution of disc height for the (pre-)ELMs (black). We have assumed the sample corresponds to 14 per cent fraction of the complete population, considering the 40 per cent rate of spectroscopic follow up for white dwarfs in SDSS (Gentile Fusillo et al. 2015) and the SDSS coverage of 35 per cent of the sky. Their distribution is consistent with the disc, assuming the scale heights for thin (300 pc) and thick disc (900 pc) given by Bland-Hawthorn & Gerhard (2016).

the disk, but there is a larger tail to high velocities than expected from a disc distribution. The same happens for the objects whose radii are inconclusive. In the case of the (pre-)ELMs, this can maybe be explained by a contribution of the orbital component to the estimated velocities, given that (pre-)ELMs are most likely of binary origin. For the remaining objects, the larger velocities could be due to a halo population. This is not unexpected, given that much of the disc population of larger stars would be above the saturation limit of the SDSS ($g \approx 14.0$). In fact, over 2100 objects in the sample (40 per cent) show tangential velocity $v_T > 200 \text{ km s}^{-1}$ (the halo selection assumed by Gaia Collaboration et al. 2018). 126 show $v_T > 500 \text{ km s}^{-1}$. Although out of the scope of this work, their nature as possible hypervelocity stars should be investigated. It is impor-

tant to emphasise again that we cannot rule out that some of these objects could be pre-ELMs, hence the high velocity objects should also be probed as pre-ELMs, regardless of radius.

Fig. 9 shows the normalized number density of the maximum difference in radial velocity between SDSS subspectra, ΔRV , for (pre-)ELMs compared to the remaining sample. The SDSS time coverage and the signal-to-noise ratio of the subspectra are not enough to claim binarity in most cases (Badenes & Maoz 2012), but it can still be noted that the (pre-)ELMs show more objects with high ΔRV , which is expected considering that they are most likely products of binary evolution. However, it is important to notice that the (pre-)ELMs are mostly fainter than the inconclusive objects (see Fig. 3), therefore this could also be due to larger spread resulting from lower signal-to-noise (S/N) spectra. We have analysed only objects whose SDSS final spectra show $S/N > 15$, but the individual subspectra can show significantly lower S/N .

4 DISCUSSION

The evolutionary origin of the sdAs has been elusive since their discovery by Kepler et al. (2016). It has always been emphasised how *Gaia* would be able to shed light on the issue. Although the problem is not yet completely resolved, we were able to identify 274 new (pre-)ELMs among the sdA population. There is, however, a 20 per cent uncertainty in this number due to lack of extinction estimates from *Gaia*. The nature of the remaining objects in the sample is still unclear, even with the *Gaia* parallaxes.

From the 1150 objects identified as most likely (pre-)ELMs by Pelisoli et al. (2018b), 233 were in our reliable π sample, and 66 were found to be indeed (pre-)ELMs. As to the 411 objects with $\log g > 5.5$ from fits to their SDSS spectra, 140 were analysed and 21 were confirmed as pre-ELMs. Some are possibly canonical mass white dwarfs, considering their position in the H-R diagram of Fig. 4. As we cannot rule out that the remaining objects are (pre-)ELMs, even if the radii are consistent with main sequence stars, the fact that not all objects were confirmed as (pre-)ELMs should not be interpreted as unpromising. It is interesting to notice, however, that most of the identified (pre-)ELMs are concentrated at low T_{eff} (see Fig. 4), contrary to our prediction in Pelisoli et al. (2018b) that they would be more common in the hot population. As the nature of most objects still remains uncertain, further conclusions on the T_{eff} as a determining factor on the evolutionary origin of the sdAs cannot be drawn. In Appendix A, we show a comparison between the distances and proper motions quoted in the work of Pelisoli et al. (2018b) compared with the updated values from *Gaia*.

It is remarkable that the position of the discovered (pre-)ELMs coincides with the region of the H-R diagram spanned by the binary evolution models of Istrate et al. (2016). This supports a binary evolution origin for the (pre-)ELMs. In fact, we have also noticed that these objects show a distribution of RV amplitudes in the SDSS subspectra shifted to higher values when compared to the other objects in the sample. Yet some show low RV dispersion, hence it cannot be ruled out that they are single. Al-

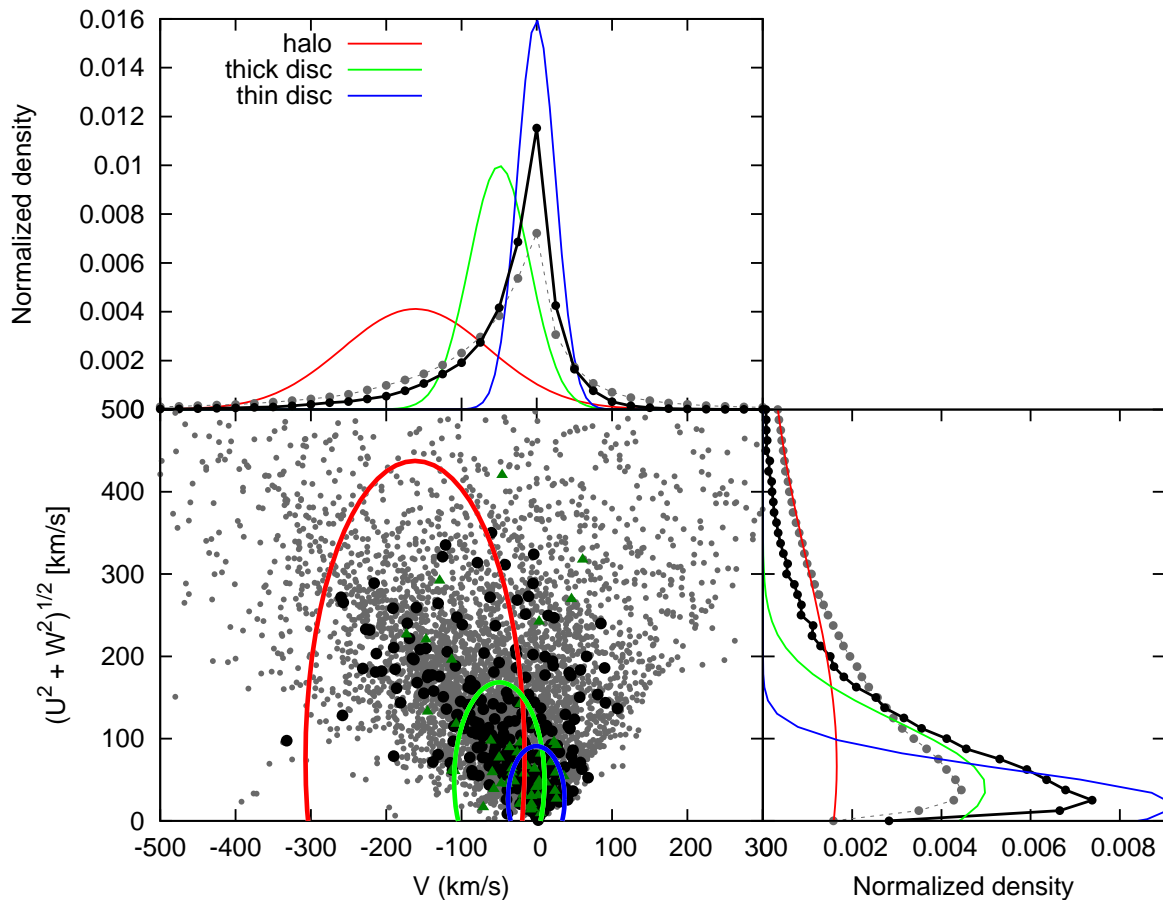


Figure 8. Bottom left panel shows the Toomre diagram following same colour coding for the dots as previous figures. The ellipsoids show the 3σ contours for Galactic thin disc (blue), thick disc (green) and stellar halo (red) populations. The top and bottom right panel show the distributions, again with same colour coding. It can be seen that the distributions peak at the position of disc, but show an extended tail. As the distances suggest that the (pre-)ELMs are within the disc, the tail could be due to an orbital component of the velocity. For the remaining objects, this could imply a halo population, given that they are detected at larger distances.

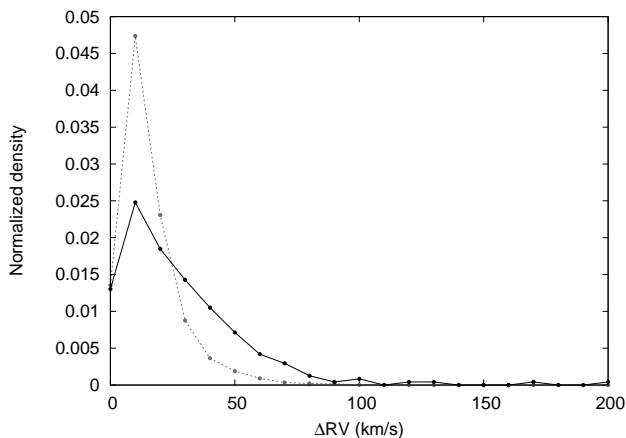


Figure 9. Normalized number density for the maximum difference in radial velocity measured in SDSS subspectra. The black line is for the identified (pre-)ELMs, the dashed grey for the remaining sample. It seems that the (pre-)ELMs show higher velocity amplitudes, as expected from a binary evolution origin.

though the (pre-)ELMs are more easily explained as having been created in multiple systems, this does not imply that they are currently in close binaries. Moreover, as mentioned in the Introduction, alternative explanations have been put forward. Time-resolved spectroscopy of the objects in this sample should be obtained so that the binary ratio of the (pre-)ELMs can be accurately determined.

As already noted in our previous works (Pelisoli et al. 2017, 2018b), the (pre-)ELM radii give the sdAs a distribution of distances consistent with the Galactic disc. The velocities are ambiguous: the peak is consistent with the disc, but the tail extends to larger velocities. This can possibly be explained by orbital motion. The remaining objects still show larger distances, with the velocities indicating that a halo contribution is required. Over a hundred of these show $v_T > 500 \text{ km s}^{-1}$ and could be high velocity stars.

The new (pre-)ELMs show temperatures cooler than the bulk of known ELMs (which mostly have $T_{\text{eff}} \gtrsim 10\,000 \text{ K}$). We have previously raised the issue of a missing, cooler population (Pelisoli et al. 2018b), and pointed out that this missing population was most likely within the sdAs, which is now confirmed.

5 SUMMARY AND CONCLUSIONS

We analysed the sample of sdAs previously published in Pelisoli et al. (2018b) in light of *Gaia* DR 2 data. The parallaxes are still uncertain ($< 3\sigma_\pi$) for 77 per cent of the sample. For the remaining 5688 objects, we verified which ones could not have a main sequence radius with a 99 per cent confidence level, finding that 274 objects are likely new (pre-)ELMs given their spectral class and radii smaller than main sequence stars. These identifications increase the number of known (pre-)ELMs by a factor of three. The majority of these new (pre-)ELMs seem to be within the disc, in contrast with the remaining sample of sdAs from SDSS that have a greater halo contribution. Moreover, the (pre-)ELMs show a distribution with higher ΔRV than the other objects, consistent with a binary evolution origin. However, the existence of single ELMs cannot be excluded.

These identifications likely correspond to only a fraction of the (pre-)ELMs within the larger sdA sample, given our conservative choice of minimal main-sequence radius. The average value of $[\text{Fe}/\text{H}]$ for the sdAs fitted by SSPP is 0.07, with a spread of 0.9, whereas we have assumed a value of $[\text{Fe}/\text{H}] = -4.0$ to determine the minimum radius. Assuming a higher metallicity would increase the minimum radius, increasing the number of objects with radii below it. On the other hand, the number of identifications decreases by 20 per cent when include an estimate of extinction based on SDSS magnitudes.

Our work demonstrates the potential of using *Gaia* to identify new (pre-)ELMs. Future data releases will further improve our understanding of the sdAs and how they fit into our theories of stellar evolution and Galaxy structure and formation. In particular, *Gaia* radial velocities from multiple epochs will enable better constraints on binarity, as would follow-up ground-based spectroscopy. Improved extinction maps would reduce uncertainties in our radius estimates, allowing us to better separate different luminosity classes. Searches independent of the SDSS identifications should be done to provide an unbiased catalogue of (pre-)ELMs (similar to the approach used to identify white dwarfs within 100 pc in *Gaia* data by Kilic et al. 2018). An unbiased catalogue could help constrain the evolutionary timescales during the pre-ELM phase compared to the cooling-track phases. The predictions from theoretical models are largely affected by uncertainties on residual burning rates. A magnitude-limited sample would also better reveal the Galactic location and kinematics of the sdA subpopulations. Such studies will not only improve our understanding of the formation of the ELMs themselves, but also of binary evolution as a whole.

ACKNOWLEDGEMENTS

IP and SOK acknowledge support from CNPq-Brazil. DK received support from programme Science without Borders, MCIT/MEC-Brazil. IP was also supported by Capes-Brazil under grant 88881.134990/2016-01. KJB was supported by the European Research Council under the European Community's Seventh Framework Programme (FP7/2007-2013) / ERC grant agreement no 338251 (StellarAges). We thank Warren Brown, Mukremin Kilic, JJ Hermes, and Saskia Hekker for reading the draft of this work and providing help-

ful comments, and Alejandra D. Romero for providing single evolution models.

This work has made use of data from the European Space Agency (ESA) mission *Gaia* (<https://www.cosmos.esa.int/gaia>), processed by the *Gaia* Data Processing and Analysis Consortium (DPAC, <https://www.cosmos.esa.int/web/gaia/dpac/consortium>). Funding for the DPAC has been provided by national institutions, in particular the institutions participating in the *Gaia* Multilateral Agreement.

REFERENCES

- Althaus L. G., Serenelli A. M., Córscico A. H., Montgomery M. H., 2003, *A&A*, **404**, 593
- Althaus L. G., Miller Bertolami M. M., Córscico A. H., 2013, *A&A*, **557**, A19
- Badenes C., Maoz D., 2012, *ApJ*, **749**, L11
- Bertelli G., Girardi L., Marigo P., Nasi E., 2008, *A&A*, **484**, 815
- Bertelli G., Nasi E., Girardi L., Marigo P., 2009, *A&A*, **508**, 355
- Bland-Hawthorn J., Gerhard O., 2016, *ARA&A*, **54**, 529
- Brown W. R., Kilic M., Allende Prieto C., Kenyon S. J., 2010, *ApJ*, **723**, 1072
- Brown W. R., Kilic M., Allende Prieto C., Kenyon S. J., 2012, *ApJ*, **744**, 142
- Brown W. R., Kilic M., Allende Prieto C., Gianninas A., Kenyon S. J., 2013, *ApJ*, **769**, 66
- Brown W. R., Gianninas A., Kilic M., Kenyon S. J., Allende Prieto C., 2016, *ApJ*, **818**, 155
- Brown W. R., Kilic M., Gianninas A., 2017, *ApJ*, **839**, 23
- Choi J., Dotter A., Conroy C., Cantiello M., Paxton B., Johnson B. D., 2016, *ApJ*, **823**, 102
- Dotter A., 2016, *ApJS*, **222**, 8
- Duchêne G., Kraus A., 2013, *ARA&A*, **51**, 269
- Evans D. W., et al., 2018, preprint, ([arXiv:1804.09368](https://arxiv.org/abs/1804.09368))
- Gaia* Collaboration et al., 2018, preprint, ([arXiv:1804.09378](https://arxiv.org/abs/1804.09378))
- Gentile Fusillo N. P., Gänsicke B. T., Greiss S., 2015, *MNRAS*, **448**, 2260
- Gianninas A., Kilic M., Brown W. R., Canton P., Kenyon S. J., 2015, *ApJ*, **812**, 167
- Hermes J. J., Gänsicke B. T., Breedt E., 2017, in Tremblay P.-E., Gänsicke B., Marsh T., eds, *Astronomical Society of the Pacific Conference Series Vol. 509, 20th European White Dwarf Workshop*. p. 453 ([arXiv:1702.07370](https://arxiv.org/abs/1702.07370))
- Istrate A. G., Marchant P., Tauris T. M., Langer N., Stancliffe R. J., Grassitelli L., 2016, *A&A*, **595**, A35
- Johnson D. R. H., Soderblom D. R., 1987, *AJ*, **93**, 864
- Jordi C., et al., 2010, *A&A*, **523**
- Kepler S. O., et al., 2016, *MNRAS*, **455**, 3413
- Kilic M., Stanek K. Z., Pinsonneault M. H., 2007, *ApJ*, **671**, 761
- Kilic M., Brown W. R., Allende Prieto C., Agüeros M. A., Heinke C., Kenyon S. J., 2011, *ApJ*, **727**, 3
- Kilic M., Brown W. R., Allende Prieto C., Kenyon S. J., Heinke C. O., Agüeros M. A., Kleinman S. J., 2012, *ApJ*, **751**, 141
- Kilic M., Hambly N. C., Bergeron P., Rowell N., 2018, preprint, ([arXiv:1805.01227](https://arxiv.org/abs/1805.01227))
- Kleinman S. J., et al., 2013, *ApJS*, **204**, 5
- Lee Y. S., et al., 2008, *AJ*, **136**, 2022
- Liakos A., 2018, preprint, ([arXiv:1805.00798](https://arxiv.org/abs/1805.00798))
- Lindgren L., et al., 2018, preprint, ([arXiv:1804.09366](https://arxiv.org/abs/1804.09366))
- Marsh T. R., Dhillon V. S., Duck S. R., 1995, *MNRAS*, **275**, 828
- Nelemans G., Tauris T. M., 1998, *A&A*, **335**, L85
- Nelemans G., Yungelson L. R., Portegies Zwart S. F., Verbunt F., 2001, *A&A*, **365**, 491
- Pelisoli I., Kepler S. O., Koester D., 2017, *Open Astronomy*, **26**, 169

- Pelisoli I., Kepler S. O., Koester D., Castanheira B. G., Romero A. D., Fraga L., 2018a, preprint, ([arXiv:1804.09059](https://arxiv.org/abs/1804.09059))
- Pelisoli I., Kepler S. O., Koester D., 2018b, *MNRAS*, **475**, 2480
- Pietrzyński G., et al., 2012, *Nature*, **484**, 75
- Postnov K. A., Yungelson L. R., 2014, *Living Reviews in Relativity*, **17**, 3
- Romero A. D., Campos F., Kepler S. O., 2015, *MNRAS*, **450**, 3708
- Schlegel D. J., Finkbeiner D. P., Davis M., 1998, *ApJ*, **500**, 525
- Tian H.-J., et al., 2017, *ApJS*, **232**, 4
- Toonen S., Hamers A., Portegies Zwart S., 2016, *Computational Astrophysics and Cosmology*, **3**, 6
- Vos J., Zorotovic M., Vučković M., Schreiber M. R., Østensen R., 2018, *MNRAS*,
- Wang B., Han Z., 2009, *A&A*, **508**, L27
- Willems B., Kolb U., 2004, *A&A*, **419**, 1057
- Zinn J. C., Pinsonneault M. H., Huber D., Stello D., 2018, preprint, ([arXiv:1805.02650](https://arxiv.org/abs/1805.02650))

APPENDIX A: COMPARISON WITH PREVIOUS DATA

Fig. A1 compares the distances obtained from the *Gaia* parallaxes with our previous values calculated from the solid angles and radii estimates. For the (pre-)ELMs, we show the distance that we derived given the radii interpolated from the models of Althaus et al. (2013) using our spectroscopic $\log g$. For a significant number of objects, the distance was underestimated by a factor of ten, which is consistent with the uncertainty of 0.5–1.0 dex that we found our $\log g$ values determined from SDSS spectra to show (Pelisoli et al. 2018a). This could also be explained if the radii inferred from the models are smaller than the actual radii, implying an underestimate of the distance. For the remaining objects, the distance was obtained assuming a radius interpolated from solar abundance main sequence models given the T_{eff} . In this case, the agreement seems better, given that our T_{eff} is reliable to 5 per cent.

In Fig. A2, we compare the proper motions used in Pelisoli et al. (2018b), obtained from the GPS1 catalogue (Tian et al. 2017) with the new estimates from *Gaia*. The proper motions agree within 3σ for 98 per cent of the sample. As we relied in proper motions, but not on the distance estimates in Pelisoli et al. (2018b), our conclusions then remain unaltered, and are in fact corroborated by this present work: the sdAs are composed of overlapping populations, and at least about 5 per cent of them are (pre-)ELMs.

This paper has been typeset from a $\text{\TeX}/\text{\LaTeX}$ file prepared by the author.

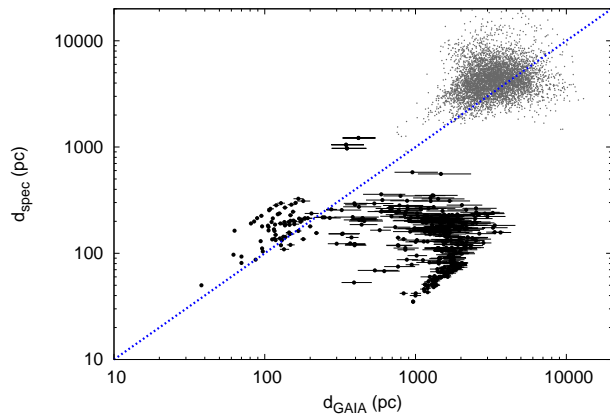


Figure A1. Comparison between the distances estimated from the spectroscopic fits and from *Gaia* parallaxes, for the (pre-)ELMs (black) and for the remaining sample (grey). For the (pre-)ELMs, the radii were estimated relying on the $\log g$, which we found to show a 0.5–1.0 dex uncertainty (Pelisoli et al. 2018a), explaining the cloud of objects with distance underestimated by a factor of ten. For the remaining objects, we show the distance obtained from the solid angle, assuming a main sequence radius interpolated given the fitted T_{eff} . There is relatively good agreement with the *Gaia* estimate in this case.

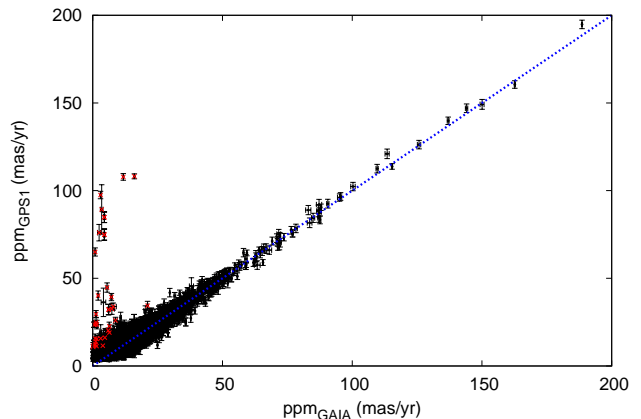


Figure A2. Comparison between the proper motions given in *Gaia* and those of the GPS1 catalogue (Tian et al. 2017), used in Pelisoli et al. (2018b). Objects marked with red crosses show proper motion different between the two catalogues to a 5σ level. Two per cent of the GPS1 proper motions for this sample are overestimated in a 3σ level.